DEVELOPMENT AND APPLICATION OF ON-LINE WELD MODELLING TOOL

W. Zhang [1] **Y-P. Yang**

Edison Welding Institute, Inc.
Columbus, Ohio (United States)

ABSTRACT

On-line software tool, E-Weld Predictor, has been developed to predict temperature, microstructure, stress, and distortion for arc welding processes by combining the power of numerical weld modelling and high performance computational hardware. It provides users with easy access to advanced modelling tools over the internet to quickly explore various welding scenarios. This paper reveals the underlying mathematical equations implemented in E-Weld Predictor and discusses several applications of E-Weld Predictor. One application is to understand the effect of heat input on the resulting microstructure, residual stresses and distortion for a U-groove X-65 steel butt joint. Results show that a larger heat input is likely to result in higher heat build-up, larger residual stresses and larger distortion. Another application is to calculate the cooling rates for a narrow groove X-100 steel weld. The results show that increase of preheating temperature reduces the cooling rate. It is hoped that by providing easy-to-use and accessible advanced weld models, the usage of the computational models will be increased by welding and design engineers in the industrial companies.

IIW-Thesaurus keywords: *Computation; Deformation; Distortion; Finite element analysis; Microstructure; Reference list; Residual stresses; Welding.*

1 INTRODUCTION

Fusion welding is a process in which an intense heat source is applied to join components. The material is rapidly heated and it melts to form a weld pool. Once the liquid pool solidifies, two parts are jointed together. The interaction between the base material and the heat source leads to a series of physical and chemical processes [1-6], which culminate in the final weld composition, geometry, and properties. In the weld region, the variation of temperature with time, often referred to as the thermal cycle, may lead to various phase transformations, changes in the grain structure, and residual stresses and distortion. Understanding the effect of fusion welding processes on the welded structure has been an important goal in the contemporary welding research [1-6].

Advances in computational software and hardware have empowered numerical models as virtual experimentation tools for improved understanding of welding processes and the resulting weld properties. The numerical weld models can be roughly classified into the following four categories: (a) heat transfer, (b) weld pool fluid flow, (c) microstructure, and (d) stress and distortion [7, 8]. The temperature variations during welding result in the changes of microstructure, stress and distortion. Heat transfer models include analytical solutions of heat conduction equation such as the classic Rosenthal equation [9] and numerical models based on finite element [10] and finite difference methods

Doc. IIW-1933-08 (ex-doc SG-212-1129r1-08) recommended for publication by SG-212 “The physics of welding”.

[1] Now Oak Ridge National Laboratory (United States).

[11]. The knowledge of thermal cycles is a prerequisite to understand the evolution of microstructure, stress and distortion during welding. The weld pool fluid flow affects the weld bead shape and size and temperature distribution in the weld metal and heat-affected zone (HAZ). The weld pool fluid flow models are typically based on finite volume method taking into account the surface tension, buoyancy and electromagnetic forces [12-15]. Additional applications of the computational fluid dynamics model include the study of arc plasma flow [16] and welding fume flow [17]. The weld microstructure models include phenomenological closed-form solutions such as Johnson-Mehl-Avarami equations [18], computational thermo-dynamics and diffusion kinetics [19], and more advanced models such as phase field and Monte Carlo simulations [20]. Finally, the stress and distortion models are based on the theory of continuum solid mechanisms [7, 8, 21]. Finite element method is typically used to calculate the welding-induced residual stresses, distortion and fracture mechanics crack driving force. An increased focus in the contemporary welding research is the integration of various models to provide a more comprehensive and detailed understanding of the welding processes.

A major challenge limiting the wider usage of weld models by industrial companies and academic research organizations is the accessibility of those models. For example, to use a finite element based stress and distortion analysis, one may have to acquire the computational software and hardware and train the staff on computational weld analysis including meshing, setting up the model and visualizing the analysis results. Such a large upfront investment in staff, technology and equipment can be cost prohibitive.

To address the model accessibility challenge, Edison Welding Institute (EWI) in collaboration with the Ohio Supercomputer Center (OSC) developed an on-line weld modelling tool (aka E-Weld Predictor [22]), which provides users with easy access to advanced predictive weld models over the internet. E-Weld Predictor allows welding and design engineers to simulate various arc welding procedure alternatives to support fabrication goals. With each calculation, the user gets a virtual prediction of the resulting microstructure, thermal profiles, residual stress, and distortion for plate and pipe welding. This paper reveals the under-the-hood mathematical equations implemented in the current E-Weld Predictor and discusses several applications.

2 APPROACH

2.1 Overview of software architecture

Figure 1 shows the architecture of E-Weld Predictor which consists of two parts: the front-end and the back-end. The user interacts with the front-end, which allows the user to define the geometry and welding procedure parameters and to view the plots after the completion of calculation. The back-end performs the finite element analysis steps automatically and does not require the user's intervention. The automatic tasks performed by the back-end include meshing, applying boundary conditions and loading conditions, solving, and generating plots. Those automatic tasks are done using user-defined PYTHON scripts developed by EWI. User subroutines based FORTRAN is used to apply the heat flux during the analysis. The back-end also contains the material property data such as yield strength at elevated temperatures for various base materials.

The simulation process flow is shown in Figure 2. As shown in this figure, a finite element mesh is automatically generated based on the user-input weld geometry. After the mesh generation, a thermal analysis is performed on the finite element mesh using ABAQUS/Standard solver. The input to the thermal model includes the welding parameters such as heat input and travel speed and thermo-physical property data such

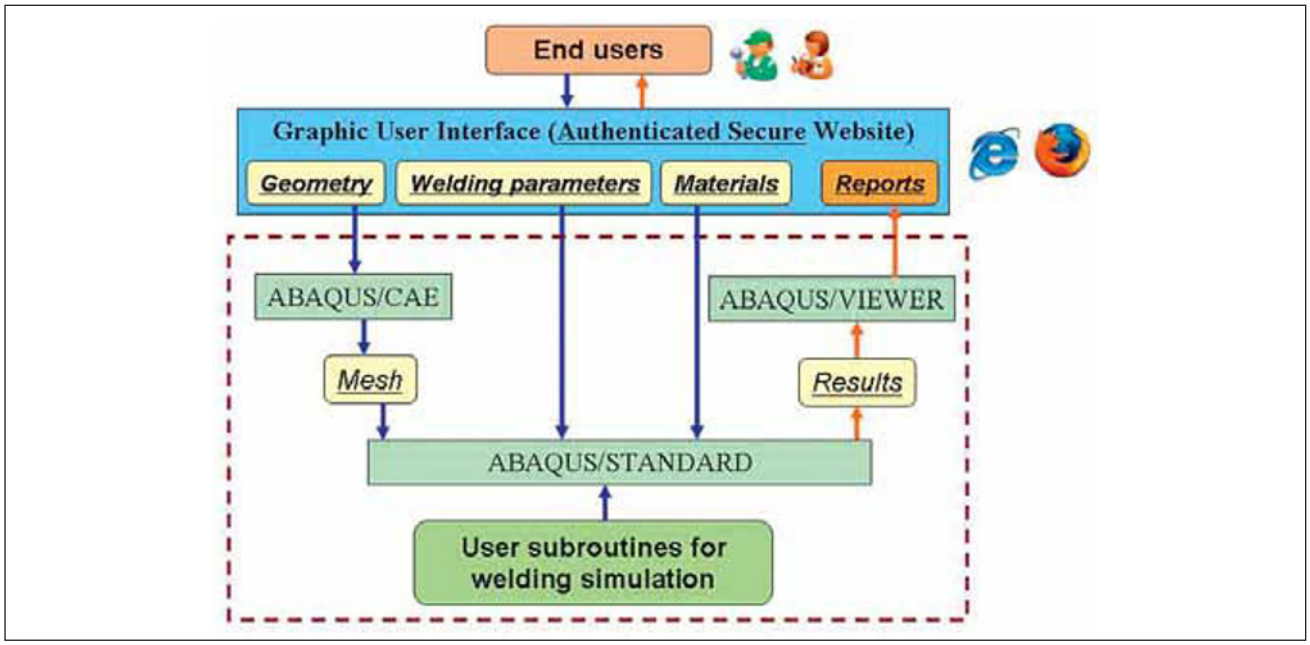

Figure 1 – Architecture of E-Weld Predictor

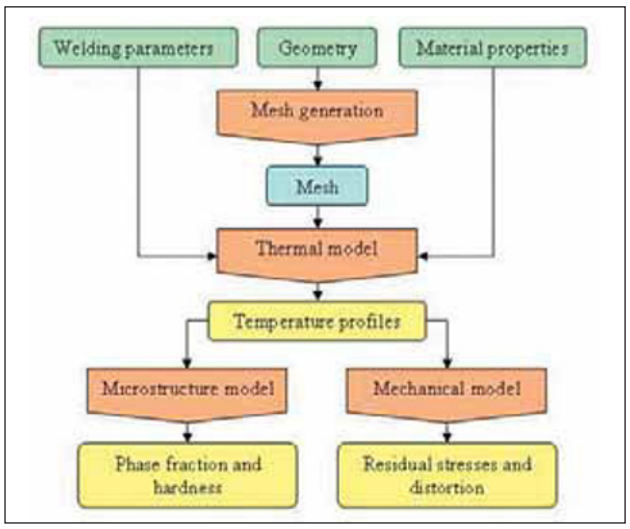

Figure 2 – Simulation process flow

as thermal conductivity and specific heat. The thermal model calculates the temperature distribution as a function of time in the entire weldment. To predict the microstructure evolution during welding, the calculated thermal profiles and material chemistry are input into the microstructure model. The predicted microstructure includes the phase fraction of final weld microstructure and a hardness map. The calculated temperature profiles are also applied as thermal loads in the mechanical model to predict the welding-induced residual stresses and distortion. Details of the above models are provided in the following sections.

2.2 Automatic mesh generation

As shown in Figure 3, the finite element weld models are based on a two-dimensional (2-D) plane perpendicular to the welding direction, i.e., the Z direction. This 2-D simplification is used to reduce the time required for the computation. A three-dimensional (3-D) analysis can take several days to complete whereas a 2-D analysis may take only a few hours. The 2-D modelling algorithm can be readily extended to the 3-D geometry.

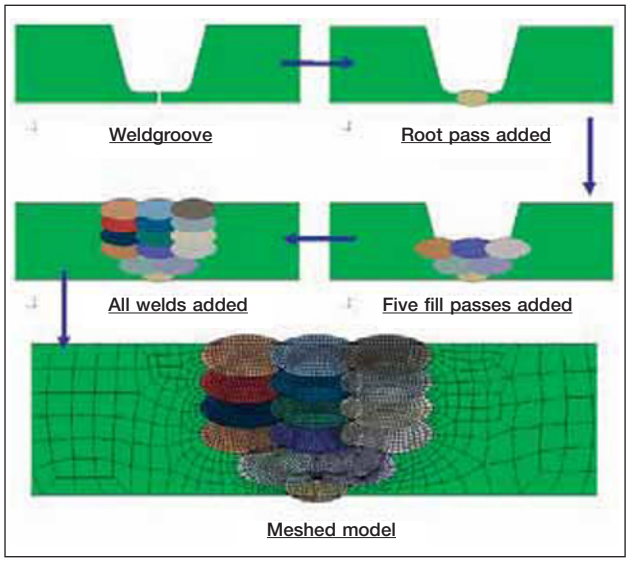

Figure 4 – Process of mesh generation

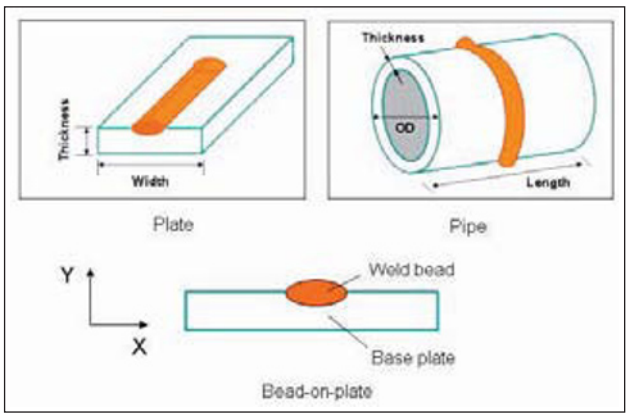

Figure 3 – 2-D plane of plate and pipe welds

As the computational hardware and software gets even more powerful, it is expected that E-Weld Predict will be able to handle the 3-D analysis.

Figure 4 shows the process of mesh generation. In the first step, the weld groove geometry is created based on the user input dimensions. In the second step, various weld passes including root, hot, fill and cap passes are deposited into the weld groove. Currently, a weld bead is approximated as an oval and the user defines the width and height of the oval, as shown in Figure 5. After all the weld passes are added, the mesh is created. As shown in Figure 4, finite element mesh for welding simulation is special since the weld area needs very fine mesh and the area far away from the weld needs to be meshed coarsely to save the computational time.

2.3 Thermal analysis

The thermal analysis is based on solution of the following transient heat conduction equation using the finite element method.

$$\rho \frac{\partial T}{\partial t} = \frac{\partial}{\partial x_i}\left(\frac{k}{C_p}\frac{\partial T}{\partial x_i}\right) + Q_v \qquad (1)$$

where

ρ is density,
T is temperature,
t is time,
k is the thermal conductivity,
C_p is the specific heat,
x_i is the distance along the i coordinate direction (i.e., X and Y), and
Q_v is the volumetric / body heat flux.

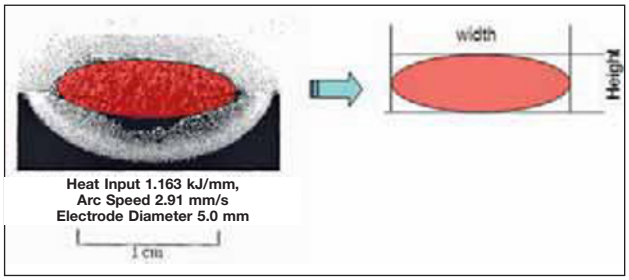

Figure 5 – Representation of a weld bead using oval shape

The heat input from the welding heat source is simulated using a combination of body heat flux and element removal and activation technique. When welding the root pass, elements belonging to all of the weld passes except the root pass are removed, as shown in Figure 6 a). A uniform body heat flux is applied to the root pass bead based on the following equation.

$$Q_v(t) = \frac{2\sqrt{3}\ \eta IV}{\sqrt{\pi}\ Ac} \exp\left(\frac{-3(z_0 + vt)^2}{c^2}\right) \quad (2)$$

where
η is the heat efficiency,
I is the welding current,
V is the voltage,
A is the area of the weld bead,
c is a geometrical coefficient,
z_0 is a distance constant, and
v is the welding speed.

Eq. (2) defines the temporary variation of the heat flux as a Gaussian function. The coefficient c is taken as 9 % of the weld bead width. After the calculation for the root pass is completed, the elements belonging to hot pass #1 are added, as shown in Figure 6 b). The uniform heat flux is then applied to the entire hot pass #1 using Eq. (2), as shown in Figure 6 c). The above steps are repeated until all the weld passes are calculated.

Convective heat loss is applied to the exterior surface of the plate using the following equation.

$$q_{loss} = h_c(T - T_a) \quad (3)$$

where
T is the surface temperature,
T_a is the ambient temperature (25 °C), and
h_c is the heat transfer coefficient
(a value of 2×10^{-5} W mm^{-2} °C^{-1} is used).

2.4 Microstructure calculation

For steel welds, the microstructure model developed by Ashby *et al*. [23] is used in E-Weld Predictor to calculate the distribution of phases such as ferrite, bainite, and martensite and the hardness map around the weld area. The carbon equivalent (CE) is a useful parameter in evaluating the influence of alloying additions on the weldability of the steel. The following equation is an empirical one recommended by the International Institute of Welding (IIW) to calculate the value of CE for a steel [23]:

$$CE = \mathrm{C} + \frac{\mathrm{Mn}}{6} + \frac{\mathrm{Cr} + \mathrm{Mo} + \mathrm{V}}{5} + \frac{\mathrm{Ni} + \mathrm{Cu}}{15} \quad (4)$$

where
C is carbon,
Mn is manganese,
Cr is chromium,
Mo is molybdenum,
V is vanadium,
Ni is nickel, and
Cu is copper.

All the composition is defined in weight percent.

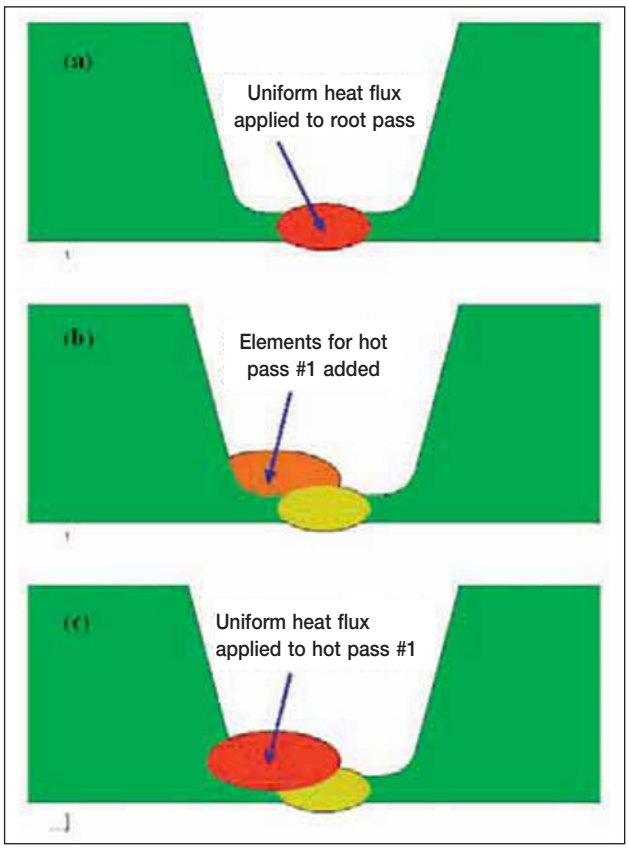

Figure 6 – Element removal and activation technique

The carbon equivalent can be used to relate to the following critical cooling rates:

$$\log \Delta t^m_{1/2} = 8.79CE - 1.52$$
$$\log \Delta t^b_{1/2} = 8.84CE - 0.74 \quad (5)$$

where
$\Delta t^m_{1/2}$ is the critical time that gives a 50 % martensite and 50 % bainite structure, and
$\Delta t^b_{1/2}$ is the time that gives a 50 % of bainite and 50 % ferrite structure.

Using the critical cooling rate, the final volume fraction of microstructure such as martensite (V_m) can be calculated as the following.

$$V_m = \exp\left\{-0.69\left(\frac{\Delta t}{\Delta t^m_{1/2}}\right)^2\right\} \quad (6)$$

where
Δt is the transformation time.

The hardness can be calculated using the following empirical equation.

$$H_m = 127 + 949\mathrm{C} + 27\mathrm{Si} + 11\mathrm{Mn} + 8\mathrm{Ni} + 16\mathrm{Cr} + 21\log V' \quad (7)$$

where
H_m is the hardness of martensite,
V' is the cooling rate at 700 °C (°C hr^{-1}).

Similar equations are available for calculating the hardness for bainite and ferrite [23]. The final hardness (H) at each point of the weld can be estimated using the rule of mixtures.

$$H = \sum H_i V_i \quad (8)$$

where

i is a particular phase, and
H_i and V_i are the hardness and volume fraction of that particular phase, respectively.

Based on the steel chemistry input from the user and the cooling rate calculated from the thermal analysis, Eq. (4) through (8) give the final volume fractions and hardness of weld microstructure.

2.5 Stress analysis

The total strain rate is given as:

$$\dot{\varepsilon}^{Tot} = \dot{\varepsilon}^{E} + \dot{\varepsilon}^{P} + \dot{\varepsilon}^{T} \quad (9)$$

where

$\dot{\varepsilon}^{Tot}$, $\dot{\varepsilon}^{E}$, $\dot{\varepsilon}^{P}$ and $\dot{\varepsilon}^{T}$ are the total, elastic, plastic and thermal strain rate tensors, respectively.

The plasticity is calculated based on the kinematic hardening model which is appropriate for metals subjected to cyclic loading [24]. The thermal strain is given as:

$$\varepsilon^{T} = \alpha(T - T_{ref}) \quad (10)$$

where

α is the coefficient of thermal expansion, and
T_{ref} is the reference temperature (25 °C).

For modelling material melting, an anneal temperature is defined for the material. Once the temperature reaches the anneal temperature, the effective plastic strain is set to zero.

The mechanical analysis is performed with ABAQUS/Standard by inputting the thermal-analysis results. Figure 7 shows the boundary conditions used in the mechanical analysis. For plate, the lower left point is fixed in the Y direction and the lower right point is fixed in both the X and Y directions. For pipe, only the lower right point is fixed in the X direction since the axisymmetric model inherently constrains the movement in the Y direction. These boundary conditions are needed to prevent the rigid body motion during the analysis of the pipe and plate weld.

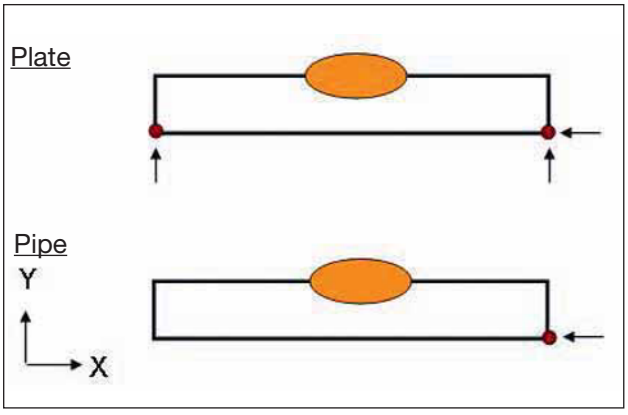

Figure 7 – Boundary conditions used in mechanical analysis

3 RESULTS AND DISCUSSION

3.1 A what-if scenario calculation

To demonstrate the practical use of E-Weld Predictor, a hypothetical case study is performed. As shown in Figure 8, two welding procedures are used to weld a U-groove butt joint with a 0.04-in. root gap and no backing plate. Procedure H uses a larger heat input of 31.4 kJ/in. and fills up the groove in 8 fill passes. On the other hand, Procedure L uses a smaller heat input of 14.6 kJ/in. and a total number of 15 fill passes is needed to fill up the groove. The base plate material is X-65 steel and the filler wire is ER70S-6. Table 1 summarizes the thermo-physical property data for the X-65 steel. Figure 9 plots the temperature-dependent mechanical property data for the X-65 steel.

Figure 10 compares the calculated temperature distribution for the two cases. As shown in this figure, the higher heat input case results in a larger HAZ than the lower heat input case. This is because the lower heat input case deposits a smaller amount of heat energy per pass, thus allowing more time for the heat to be conducted away. On the other hand, a larger amount of heat energy is deposited in the higher heat input case, resulting more extensive heat build-up near the weld area.

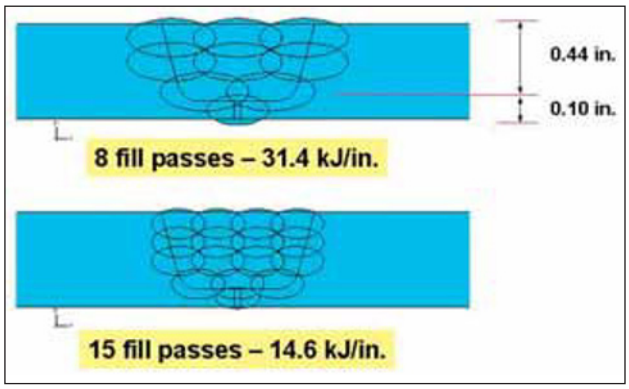

Figure 8 – Gas Metal Arc Welding of a U-groove butt-joint

Table 1 – Thermo-physical property data of the X-65 steel

Property name	Value
Density, ρ, (kg mm^{-3})	7.84×10^{-6}
Liquidus temperature (°C)	1 545
Solidus temperature (°C)	1 475
Latent heat of fusion, L, (J kg^{-1})	2.4×10^{5}
Thermal conductivity k (W mm^{-1} K^{-1})	0.037
Specific heat, C_p, (J kg^{-1} °C^{-1})	690
Heat efficiency, η	0.82
Coefficient of thermal expansion, α, (mm mm^{-1} °C^{-1})	1.2×10^{-5}

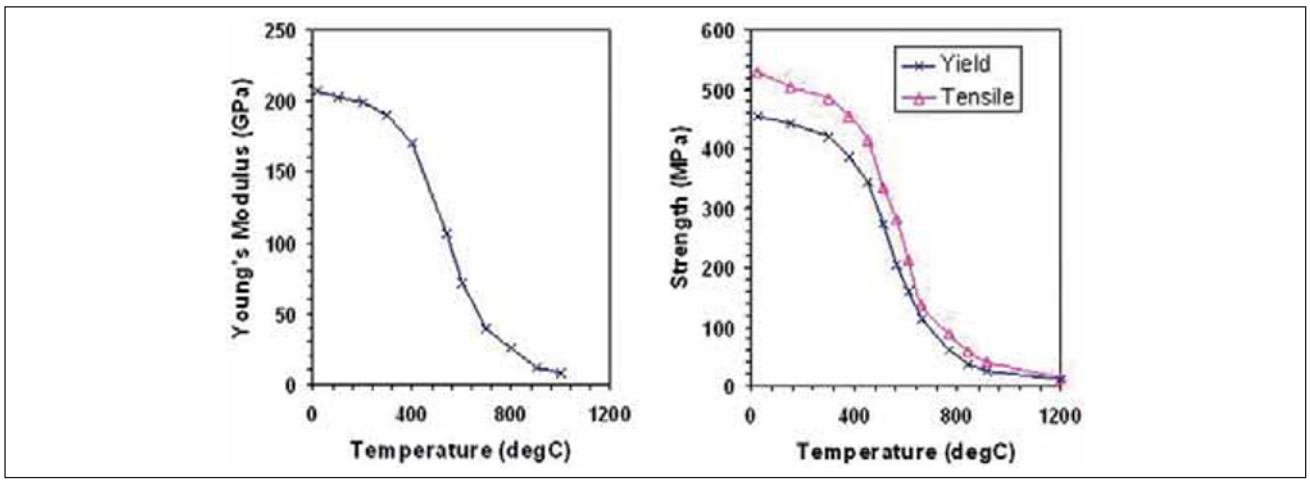

Figure 9 – Temperature-dependent mechanical property data of X-65 steel

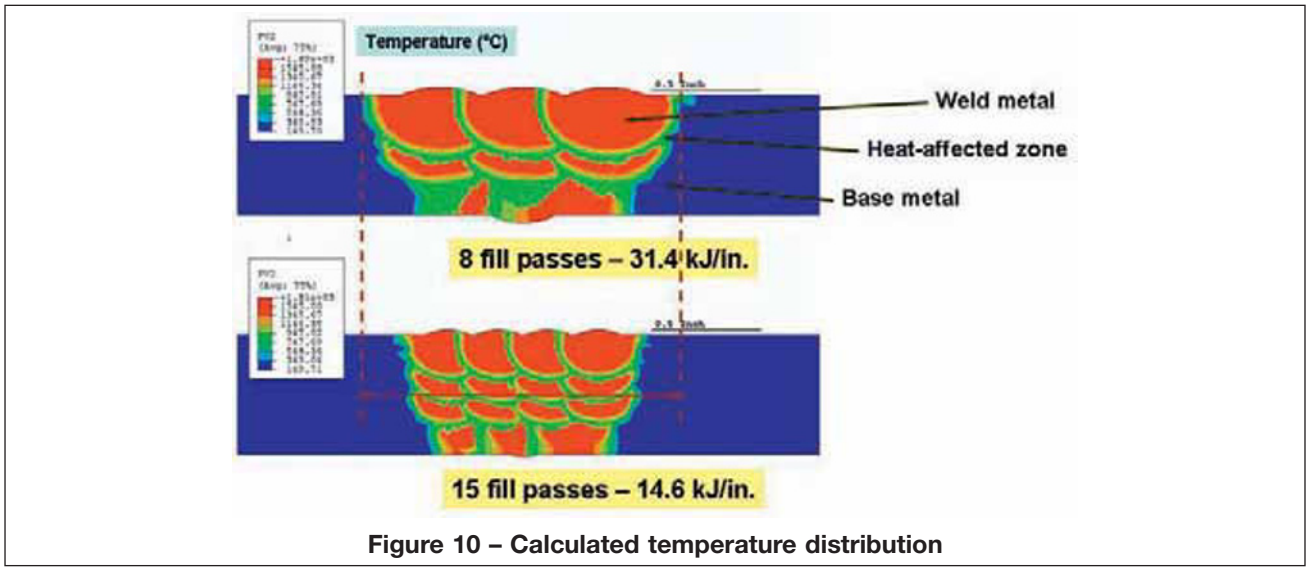

Figure 10 – Calculated temperature distribution

The hardness map for the two cases is plotted in Figure 11. The peak hardness for the smaller heat input case is higher. This is expected since the smaller heat input results in a faster cooling rate. Faster cooling favours the formation of harder phases such as martensite.

The residual stresses and distortion for the two cases are shown in Figure 12 and Figure 13, respectively.

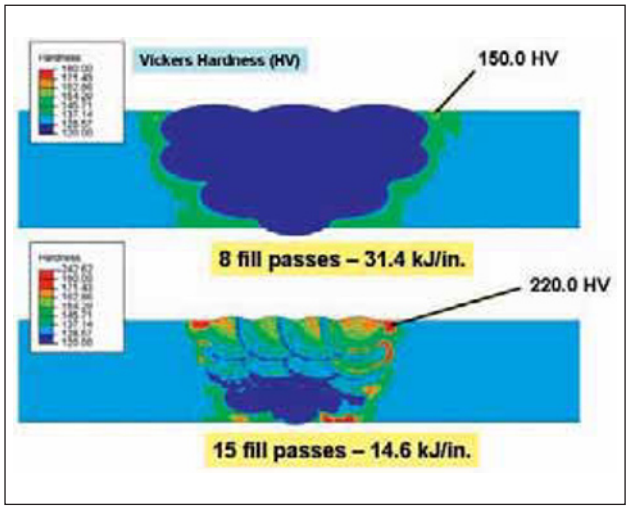

Figure 11 – Calculated hardness distribution

Table 2 summarizes the peak stress and angular distortion for the two cases. The higher heat input case leads to a larger heat-affected area. As a result, larger residual stress and distortion are observed when the higher heat input is used.

In summary, the results of the above case study indicates that a higher heat input, while being more produc-

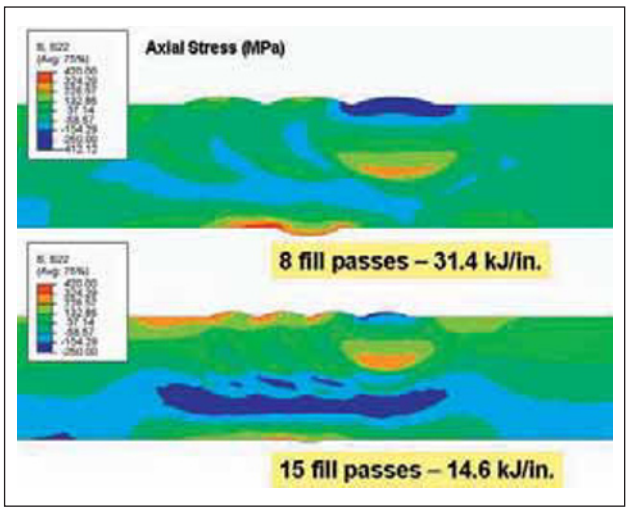

Figure 12 – Calculated welding residual stress – Axial stress

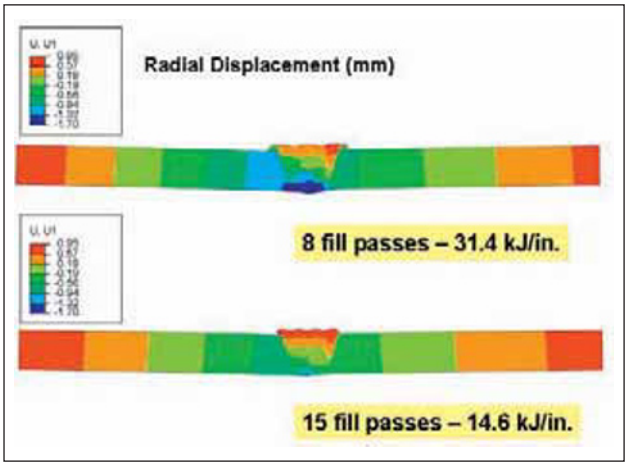

Figure 13 – Calculated welding distortion – Radial displacement

Table 2 – Effects of heat input on the hardness, residual stress and distortion

	Larger heat input	Smaller heat input
Number of fill passes	8	15
Heat input per pass (kJ/in.)	31.4	14.6
Hardness (HV)	150.0	220.0
Peak axial tensile stress (MPa)	408.0	336.0
Angular distortion (degree)	0.93	0.87

tive, can result in higher heat build-up, residual stresses and distortion. A trade-off consideration may be needed to balance the productivity and resulting weld properties. E-Weld Predictor is a useful tool for such quick what-if scenario calculation.

3.2 Calculation of cooling rates for X-100 steel welds

Figure 14 compares the macrograph and the model representation of a narrow groove weld [25]. In the current E-Weld Predictor, the dimensions (i.e., width and height) are required to be the same for all the individual fill and cap weld beads. Due to this limitation, the simulated fill passes #1 and 2 has a larger bead width than the width of the groove.

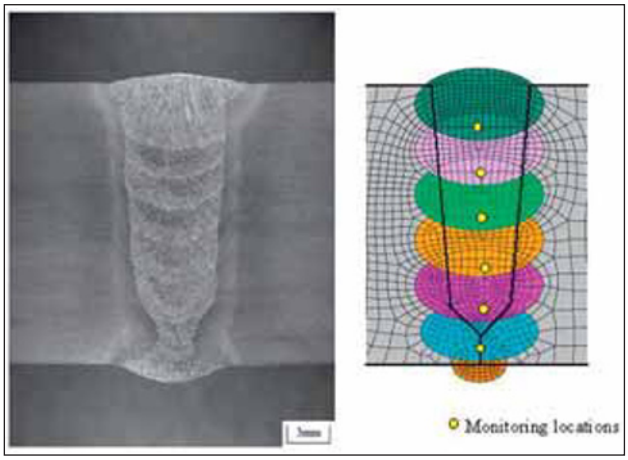

Figure 14 – Macro of a narrow groove weld and the corresponding 2-D model

Figure 15 compares the measured and predicted cooling rates from 800 to 400 °C for cases with different preheating temperatures. As shown in this figure, the

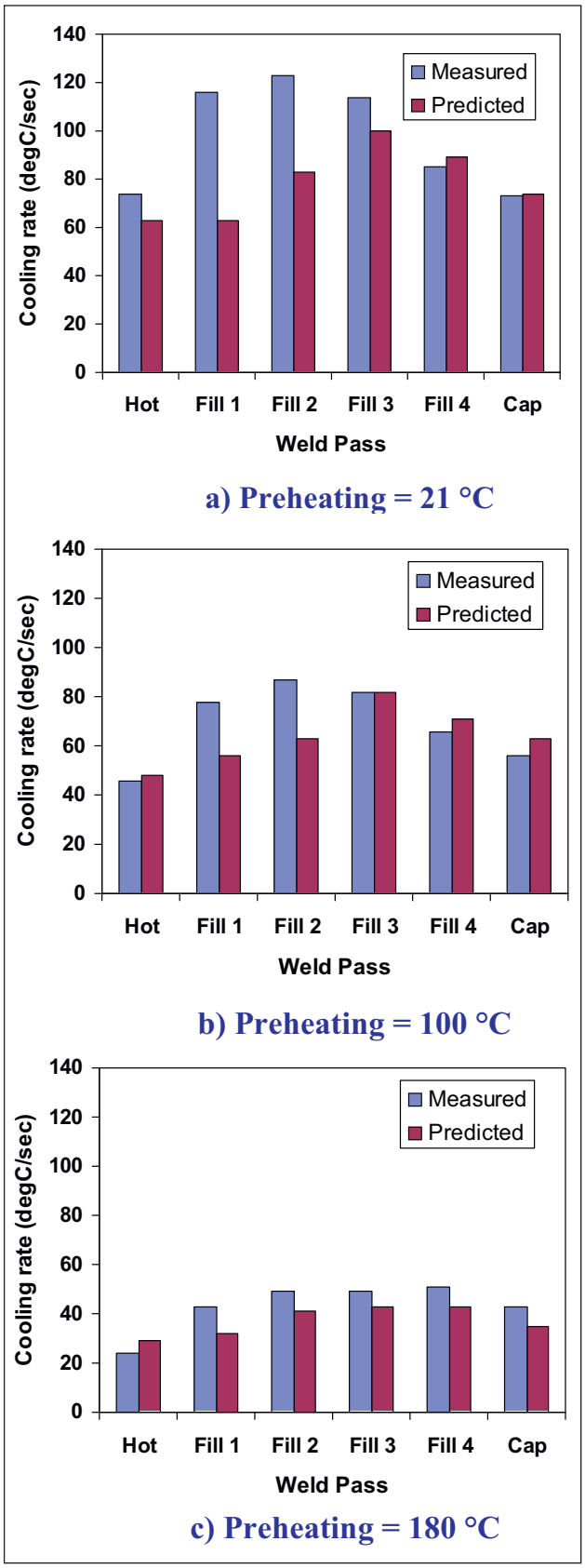

Figure 15 – Comparison between measured and predicted cooling rates from 800 to 400 °C

model tends to under-predict the cooling rate. The maximum error between the predicted and measured cooling rate is 47 % for the preheating temperature of 21 °C. The accuracy of the model prediction improves as the preheating temperature increases. The model correctly predicts the effect of the preheating temperature on the cooling rate, i.e., the higher the preheating temperature, the lower the cooling rate. A major reason for the discrepancy between the calculated and measured cooling rates is that the oval shape is less than adequate for representing the weld bead shape in the narrow groove weld.

3.3 Weld bead shape and pass sequencing

As discussed earlier, a major simplification in the current E-Weld Predictor is the representation of the weld bead shape by an oval. To address this simplification, a general weld meshing algorithm is developed. Figure 16 illustrates the digitization of a weld bead contour into a series of XY coordinates. The digitization is done by importing the weld macrograph into an image editing software and recording the XY coordinates of the visible weld bead boundary. The general weld meshing algorithm imports the weld bead profile coordinates and automatically generates a mesh for the finite element analysis. Figure 17 shows an application of the general weld meshing algorithm. As shown in this figure, the grey area (above 1 500 °C) is assumed to represent the weld metal while the red area (between 1 250 and 1 500 °C) is assumed to represent the coarse-grain HAZ. The predicted microstructure map is consistent with that observed in the weld macro.

4 SUMMARY AND CONCLUSIONS

By combining the power of high performance computational hardware, finite element analysis software, and numerical weld modelling, an on-line software tool, E-Weld Predictor has been developed to predict temperature, microstructure, stress, and distortion during arc welding processes. This software tool implements automatic modelling tasks without the user's intervention based on customized scripts and user-subroutines. Those automatic modelling tasks include mesh generation, model set up, thermal analysis, microstructure analysis, mechanical analysis and visualization of analysis results. E-Weld Predictor is easily accessible; it can be accessed from a personal computer with an Internet connection from anywhere in the world. This helps minimize the upfront investment in computational hardware and software and technology typically associated with numerical simulation.

The case studies reported in the present paper demonstrates that E-Weld Predictor is a powerful tool for the simulation of various arc welding procedures.

– The effect of heat input was studied by evaluating the resulting microstructure, residual stresses and distortion for two different heat input levels. It is found that a higher heat input is likely to result in higher heat build-up and larger residual stresses and distortion.

– For a narrow groove weld, the cooling rates were calculated for various preheating temperatures. An increase of preheating temperature reduces the cooling rate.

– A general meshing algorithm was used to model the actual weld bead profile and pass sequencing. Predicted microstructure distribution was consistent with that observed experimentally for a multi-layer and multi-bead steel weld.

It is hoped that by providing easy-to-use and accessible advanced weld models, the usage of the computational models will be increased by welding and design engineers in the industrial companies.

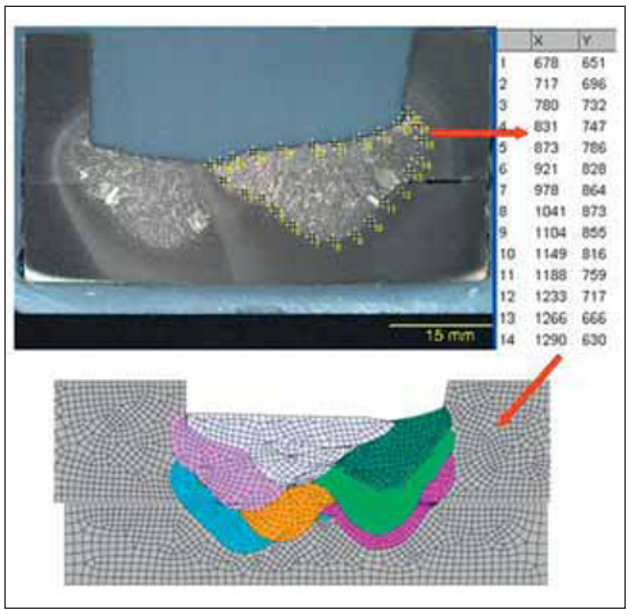

Figure 16 – Digitizing of weld bead profile and automatic generating finite element mesh

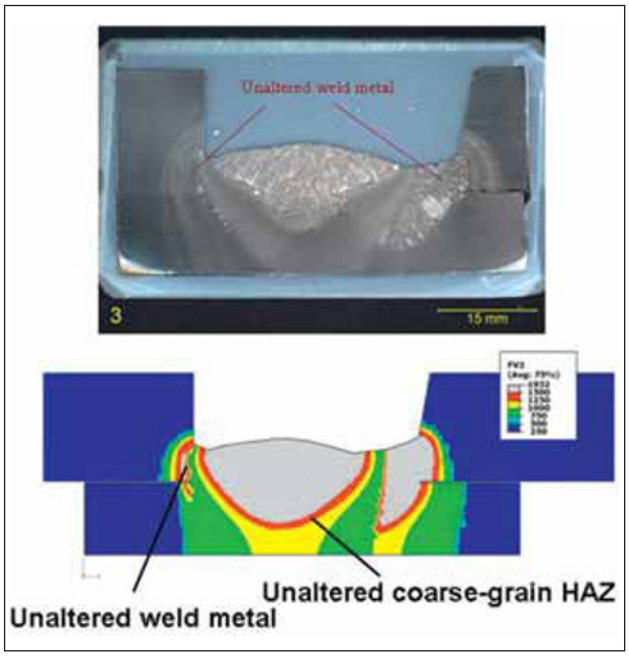

Figure 17 – Predicted temperature distribution for a steel weld

5 FUTURE DEVELOPMENT

Additional new enhancements are constantly added to E-Weld Predictor. The future development includes the development of a weld bead profile databank which correlates the welding procedure parameters to the weld bead shape. New joint geometry such as T-joint is planned to be developed. Microstructure predictions will be enhanced to calculate the HAZ softening and inter-pass tempering for steel welds. New microstructure models will be added for titanium alloys.

As a vehicle for delivering advanced models to industrial users, the usefulness and value of E-Weld Predictor will be greatly enhanced by incorporating a suite of weld models into it. Interested parties are welcome to discuss the possibility for porting their modelling applications to E-Weld Predictor.

ACKNOWLEDGEMENTS

EWI acknowledges the contribution of the State of Ohio, Department of Development and Thomas Edison Program, which provided funding in support of Edison Technology and Industry Center Services. The content reflects the views of EWI and does not purport to reflect the views of the State of Ohio. The authors are grateful to Dr. S. S. Babu, J. Xu, W. Gan, S. P. Khurana and C. Conrardy for their support. The authors also sincerely thank Ohio Supercomputer Center for implementing of the front-end and hosting the E-Weld Predictor.

REFERENCES

[1] Lancaster J.F.: The Physics of Welding 2nd Edition, Pergamon, Oxford, 1986.

[2] Easterling K.E.: Introduction to the Physical Metallurgy of Welding, 2nd Edition, Butterworth-Heinemann, Oxford, 1992.

[3] David S.A., DebRoy T.: Science, 1992, 257, 497.

[4] DebRoy T., David S.A.: Rev. Mod. Phys., 1995, 67, 85.

[5] Grong Ø.: Metallurgical Modeling of Welding, 2nd edition, The Institute of Materials, London, 1997.

[6] Kou S.: Welding Metallurgy, 2nd edition, John Wiley & Sons, Hoboken, New Jersey, 2003.

[7] Goldak J.A., Akhlaghi M.: Computational Welding Mechanics, Springer, New York, 2005.

[8] Lindgren L.-E.: Journal of Thermal Stress, 2001, 141, 24.

[9] Rosenthal D.: Transactions of the ASME, 1946, 849, 43.

[10] De A., Maiti S.K., Walsh C.A., Bhadeshia H.K.D.H.: Science and Technology of Welding and Joining, 2003, 377, 8.

[11] Kim C.-H., Zhang W., DebRoy T.: J. Appl. Phys., 2003, 94, 2667.

[12] Zhang W., Roy G.G., Elmer J.W., DebRoy T.: J. Appl. Phys., 2003, 93, 3022.

[13] Cao Z., Yang Z., Chen X.L.: Welding Journal, 2004, 169-S, 83.

[14] Zhang W., Kim C.-H., DebRoy T.: J. Appl. Phy., 2004, 5210, 95.

[15] Cho M.H., Farson D.F.: Metallurgical and Materials Transactions B, 2007, 305, 38.

[16] Lago F., Gonzalez J.J., Freton P., Gleizes A.: Journal of Physics D, 2004, 883, 37.

[17] Godbole A., Cooper P., Norrish J.: Australasian Welding Journal, 2007, 35, 52.

[18] Elmer J.W., Palmer T.A., Zhang W., Wood B., DebRoy T.: Acta Materialia, 2003, 3333, 51.

[19] Zhang W., DebRoy T., Palmer T.A., Elmer J.W.: Acta Materialia, 2005, 4441, 53.

[20] Mishra S., DebRoy T.: Acta Materialia, 2004, 1183, 52.

[21] Yang Y.P., Dong P., Zhang J.: Welding Journal, 2000, 9-S, 79.

[22] http://www.calculations.ewi.org/vjp/

[23] Ion J.C., Easterling K.E., Ashby M.F.: Acta metall., 1984, 1949, 32.

[24] ABAQUS Analysis User's Manual, Version 6.7, Dassault Systems, 2007.

[25] Hudson M.G.: Welding of X100 Linepipe, Ph.D. Thesis, Cranfield University, 2004.